JOURNAL OF SOLID STATE CHEMISTRY 75, 332–346 (1988)

Magnetism and Superconductivity in the Spinel System $Li_{1-x}M_xTi_2O_4$ ($M = Mn^{2+}, Mg^{2+}$)

P. M. LAMBERT*

Baker Laboratory of Chemistry, Cornell University, Ithaca, New York 14853

M. R. HARRISON

GEC Research Limited, Hirst Research Centre, East Lane, Wembley, Middlesex HA9 7PP, United Kingdom

AND P. P. EDWARDS†

Superconductivity Research Centre, University of Cambridge, University West Cambridge Site, Madingley Road, Cambridge CB3 0HE, and University Chemical Laboratory, Lensfield Road, Cambridge CB2 1EW, United Kingdom

Received February 2, 1988, in revised form February 19, 1988

X-ray powder diffraction measurements show that the M^{2+} cations substitute almost completely at the tetrahedral sites in the $Li_{1-x}M_xTi_2O_4$ spinel systems ($M = Mn^{2+}$, $0 < x < 1$; $M = Mg^{2+}$, $0 < x < 0.2$). The magnetic susceptibility of the $Li_{1-x}M_xTi_2O_4$ system is dominated by high-spin Mn^{2+} moments for $x < 0.5$ and shows ferrimagnetic ordering at low temperatures (15–55 K) for samples with higher x compositions. The occurrence of spontaneous magnetism in the $Li_{0.4}Mn_{0.6}Ti_2O_4$ sample is interpreted as indicating a compositionally induced metal–nonmetal transition near that composition. The titanium–titanium cation distance at the transition is 3.016(2) Å in excellent agreement with Goodenough's critical R_c value of 3.02 Å for Ti^{3+} ions. The magnetic susceptibility of the $Li_{1-x}Mg_xTi_2O_4$ system is distinguished by large Pauli susceptibilities and the Curie behavior of small concentrations of spins trapped at defect sites. The superconducting transition temperature T_c falls with increasing x and shows a strong correlation with the lattice parameter in both series. A decreasing density of states at the Fermi level resulting from increasing electron correlation and electron–lattice interactions is proposed to account for these observations. Importantly, no magnetic impurity effect on T_c is observed.

Introduction

The $Li_{1+x}Ti_{2-x}O_4$ ($0 < x < \frac{1}{3}$) spinel system was originally synthesized and structurally characterized by Deschanvres *et al.* (*1*). Subsequent investigations revealed the end member $LiTi_2O_4$ to be a high-temperature superconductor with a transition temperature $T_c \approx 11$ K (*2–5*). The compositional range of the solid solution spans a titanium valency of +3.5 in $LiTi_2O_4$ to +4 in $Li_{4/3}Ti_{5/3}O_4$ and the latter compound is an electrical insulator. Thus a composition-

* Present address: Eastman Kodak Co., Research Laboratories, Rochester, NY 14650.

† To whom correspondence should be addressed.

0022-4596/88 $3.00

ally induced metal–nonmetal transition (MNMT) is inescapable within the homogeneity range. The position of the MNMT, as suggested by an increase in the pressed-pellet electrical resistivity and a reduction in the Pauli susceptibility, is placed at $x = 0.1$–0.15 and is distinguished by a complete loss of superconductivity (*4*, *6–8*). Prior to the transition, T_c remains virtually constant.

X-ray diffraction studies show that the spinel tetrahedral *A* sites in the $Li_{1+x}Ti_{2-x}O_4$ series are occupied by lithium cations and the octahedral *B* sites are randomly populated by titanium and lithium ions in the ratio determined by the composition (*4*). The electronic and magnetic properties are attributable to the titanium 3*d* electrons. The direct cation–cation orbital overlap between adjacent edge-sharing octahedra in the spinel structure forms a conduction band composed largely of the titanium 3*d* t_{2g} orbitals. A schematic band structure (Fig. 1) shows the titanium 3*d* orbital manifold to be split by the cubic crystal field into an empty e_g band and a partially filled t_{2g} conduction band (1/12 full in $LiTi_2O_4$). Ideal cubic close packing is seldom realized in the spinel structure and the anions are usually distorted along the ⟨111⟩ direction in order to accommodate the different cation radii in the *A* and *B* sites. The effect, described by the oxygen positional parameter *u*, superimposes a slight trigonal distortion at the octahedral site as shown in Fig. 1.

Magnetic susceptibility and electron spin resonance measurements (*7*) show the presence of a small number (1–2 mole%) of localized moments in all but the $x = \frac{1}{3}$ composition which are apparently associated with oxygen vacancies. The $Li_{1+x}Ti_{2-x}O_4$ system has also been the subject of photoelectron (*9*) and diffuse reflectance (*10*) spectroscopy studies.

The existence of metallic behavior and superconductivity in $LiTi_2O_4$, combined with the relative ease of cation substitution in the spinel structure, offers the unique opportunity to effect metal–nonmetal transitions and to manipulate the superconducting properties in a systematic manner. In this paper, we describe the results of experiments in which cation substitution on the spinel tetrahedral sublattice is performed where Li^+ is replaced by Mn^{2+} or Mg^{2+}. In a subsequent paper, substitution of titanium cations on the octahedral sublattice by Cr^{3+} or Al^{3+} will also be presented. Each type of sublattice substitution manipulates lattice expansion and electron concentration in the opposite sense and each pair of sublattice substitutions offers the valuable additional comparison of magnetic versus nonmagnetic dopants. In this way, the effects of octahedral and tetrahedral substitution on properties such as superconductivity and the MNMT can be distinguished.

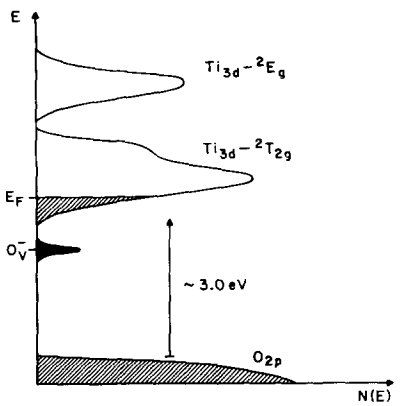

FIG. 1. Schematic band structure of a metallic composition in $Li_{1+x}Ti_{2-x}O_4$. Localized oxygen vacancy states are indicated by O_V^-.

Experimental

Powder samples were prepared through the solid-state reaction of the component oxides in a manner similar to that of Johnston (*4*) and Harrison *et al.* (*7*). Stoichiometric amounts of Li_2CO_3 (atomergic,

99.99%), TiO_2 (AESAR, 99.9998% Puratronic), Ti_2O_3, and either MgO (CERAC, 99.95%) or MnO (CERAC, 99.9%) were mixed and fired according to the overall reaction,

$$(1 - x)Li_2CO_3 + 2xMO + 2(1 - x)TiO_2 + (1 + x)Ti_2O_3 \rightarrow 2Li_{1-x}M_xTi_2O_4 + (1 - x)CO_2, \quad (1)$$

where M is Mg or Mn. The Ti_2O_3 was prepared from Ti metal (AESAR, 99.99%) and TiO_2 at 1600°C under RF heating and checked for stoichiometry by oxidation. The phase purity of the dried starting materials was verified by X-ray diffraction measurements.

The oxidized components for each composition were intimately mixed in an agate mortar for 10–15 min, pressed in ½-in.-diameter pellets at 25,000 psi and fired at 750°C for 2½ hr. This "prefiring" promoted cation mixing on an atomic scale; without this step, samples usually contained the impurity phase described by Harrison *et al.* (*8*) and Inukai and Murakami (*11*). The duration of the prefiring encouraged complete loss of CO_2 (to within 0.5% of theoretical loss). The prefiring temperature was limited to 750°C to avoid the loss of lithium oxide.

The prefired pellet was ground with the required amount of Ti_2O_3 for 30–40 min either in an inert atmosphere (VAC Helium Dri-Lab) or in air; no differences in the final sample properties were observed between the two preparations. The powder mixtures were again pressed into ½-in. pellets at 25,000 psi.

Sample tubes were prepared from fused quartz tubing (Hereaus-Amersil Inc. 12-mm OD × 1-mm wall) and were washed with aqua regia, rinsed in distilled deionized water, then dried and degassed for 1 hr under vacuum (10^{-5} Torr) at 1000°C.

The pellets were wrapped in 0.001-in. OFHC copper foil to reduce lithium loss through diffusion into the silica walls of the sample tube. No reaction was observed between the sample pellets and the copper foil. After sealing under vacuum (10^{-5} Torr), the samples were placed in a box furnace at 500–600°C. The temperature was then raised over the course of 2–3 hr to the final firing temperature, held there for 16–18 hr, and allowed to cool to ambient temperature. The firing temperatures varied linearly with x from 850°C for $x = 0.0$ to 1190°C for $x = 1.0$. Higher firing temperatures for low values of x were not possible because of the structural transformation to the ramsdellite phase (*12*).

Debye–Scherrer X-ray powder diffraction patterns were obtained for all samples using 114.6-mm-diameter cameras and nickel-filtered Cu$K\alpha$ radiation. The method of lattice parameter determination has been previously described (*13*). Powder diffractometer tracings were obtained either with an Enraf–Nonius diffractometer equipped with a Stoe Bragg-Brentano goniometer (NRC Laboratory, Ottawa, Canada) or with a Philips diffractometer (University Chemical Laboratory, Cambridge, England).

The integrated peak intensities obtained from the diffractometer tracings were normalized to 1000 and used to determine u, the oxygen parameter for the spinel structure, and the cation site distributions for several samples using the Furuhashi method (*14*). The technique describes the diminution of the line intensity with increasing θ by means of an effective temperature factor B_{eff}. The best structure is that which gives the best linearity for the relation,

$$\ln(I_{\text{obs}}/I_{\text{calc}}) = \ln K - 2B_{\text{eff}}(\sin^2\theta/\lambda^2), \quad (2)$$

where K is a scale factor, λ is the X-ray wavelength, and

$$I_{\text{calc}} = |FF^*|Lpm, \quad (3)$$

where F is the calculated structure factor, L is the Lorentz factor, p is the polarization

factor, and m is the multiplicity of the reflection. The absorption correction factor was ignored in the calculated intensity as the linear absorption coefficient was assumed to be large.

Intensity calculations were performed by the LAZY PULVERIX program (*15*) for various site distributions and values of u. The calculated intensities were compared with between 9 and 15 observed lines of sufficient intensity ($I_{obs} > 5$) using Eq. (2). The degree of linearity was judged by the magnitude of the root-mean-square standard deviation of a linear least-squares fit between $\ln(I_{obs}/I_{calc})$ and $\sin^2\theta/\lambda^2$. For each fit, B_{eff} and K were determined. The most probable structure was determined via a heuristic grid search in the u and cation distribution space in which lithium and oxygen nonstoichiometries were also considered.

Static magnetic susceptibility measurements were obtained by the Faraday method on a computer-interfaced instrument described previously (*16*). Calibration was performed using $HgCo(SCN)_4$ as a standard. Magnetization curves were calculated from the approximate applied fields of 8400 G and 12,000 G. Spontaneous magnetization curves were estimated by extrapolation to zero field. The magnetic ordering temperatures were taken as the low-temperature inflection points of the inverse susceptibilities. The temperature-independent Van Vleck paramagnetism of Ti^{4+} in an oxygen octahedra nearly compensates for the core diamagnetism in all samples (*4*); therefore, core corrections were not applied to the susceptibilities.

Superconducting transition temperatures were determined by the AC mutual inductance technique on an instrument described earlier (*16*). Transition temperatures are reported at 50% of full signal deflection and transition widths at between 10 and 90% deflection.

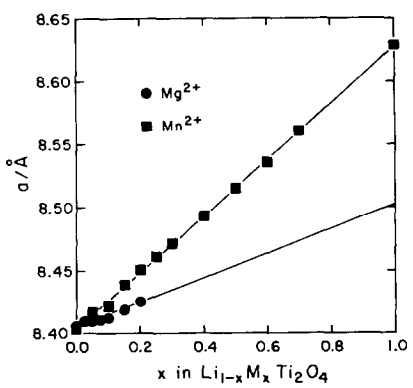

FIG. 2. Cubic lattice parameter a for $Li_{1-x}M_xTi_2O_4$; $M = Mn^{2+}, Mg^{2+}$.

Structural Parameters

Single-phased polycrystalline samples of $Li_{1-x}Mg_xTi_2O_4$ systems were prepared up to $x = 0.2$; beyond this composition unreacted Ti_2O_3 was present as a major impurity. The linear compositional dependence of the cubic lattice parameter is

$$a = (8.4046 + 0.0967x)\ \text{Å} \qquad (4)$$

with a correlation coefficient of 0.979 (Fig. 2).

Lecerf (*17*) described a laborious preparation of $MgTi_2O_4$ in which a 0.7/1.0 mixture of MgO and TiO_2 was stoichiometrically reduced with acetylene black at 1400°C in argon. The reaction product consisted of a cubic phase and MgO, the latter which was dissolved in dilute HCl. X-ray analysis showed the cubic phase to be a normal spinel with a lattice parameter $a = 8.474(2)$ Å. Johnston (*3*) also claimed to have prepared $MgTi_2O_4$ with a lattice parameter of 8.505(3) Å, but provided no synthetic details. Studies of nitrogen-fixing Mo/Ti/Mg hydroxides (*18*) claimed that $MgTi_2O_4$ was formed by coprecipitation with alkali from a methanolic solution of $MgCl_2$ and $TiCl_3$. Two phases were formed; a nearly amorphous material and a cubic phase considered to be $MgTi_2O_4$ despite the large lattice parameter of 8.9 Å. The precip-

itate was rapidly oxidized on exposure to air.

Reaction of MgO and Ti_2O_3 in sealed evacuated tubes, or by RF heating in vacuum, was incomplete, and nearly a 50% excess of MgO was required to consume the Ti_2O_3 and produce a single-phase spinel. The lattice parameter of this material is 8.502(2) Å, close to Johnston's reported value for $MgTi_2O_4$.

Polycrystalline powder samples of the $Li_{1-x}Mn_xTi_2O_4$ series were prepared for $0.0 < x < 1.0$. The color of the samples varies smoothly from royal blue for $LiTi_2O_4$ ($x = 0.0$) to black for $MnTi_2O_4$ ($x = 1.0$). All diffraction lines in the Debye–Scherrer powder patterns were indexed to a cubic system with extinctions consistent with the spinel space group. No superstructure lines are evident. A linear dependence of the cubic lattice parameter a with x is seen in accordance with Vegard's law (Fig. 2). The composition dependence is

$$a = (8.404 + 0.223x) \text{ Å} \qquad (5)$$

with a correlation coefficient of 0.999. The average lattice parameter of the three $LiTi_2O_4$ samples is 8.405(2) Å and is consistent with the reported ceramic preparations (*4, 7, 19, 20*).

All samples were predominately single-phased; the $x = 0.7$ and 1.0 compositions contain traces of unreacted Ti_2O_3 (~5%). A $x = 0.85$ sample was prepared and was found to contain a significant amount of Ti_2O_3. In this compositional range, higher reaction temperatures are likely to be required for a single-phase spinel product. However, the concomitant increase in Li_2O loss would be undesirable.

Lecerf (*17*) first claimed to have produced stoichiometric $MnTi_2O_4$ through the solid-state reaction of a sixfold excess of Mn metal and TiO_2 fired at 1400°C in argon. The excess Mn was subsequently removed with dilute hydrochloric acid. The reported cubic lattice parameter is 8.600(2) Å. A second $MnTi_2O_4$ preparation by Lecerf was less severe; a stoichiometric mixture of Mn and TiO_2 was fired in argon at 1200°C, cooled, ground, and refired (*21*). The reported lattice parameter is 8.628(2) Å in excellent agreement with the $x = 1.0$ sample. Presumably the smaller unit cell of original synthesis reflected the effects of acid leaching.

The cation site distributions, oxygen parameters, and temperature factors obtained from the line intensity analysis of the powder diffractometer tracings are compiled in Table I, and comparisons of theoretical intensities (adjusted by B_{eff} and the scale factor K) and the observed intensities are shown in Table II.

In all the compositions analyzed, the M^{2+} ion appears to substitute for lithium largely at the tetrahedral sites, thus maintaining the integrity of the titanium octahedral sublattice. For intermediate value of x in the manganese series the presence of a slight amount of Li^+ on the octahedral sites is indicated, and for the $x = 0.15$ sample of the

TABLE I

CATION SITE DISTRIBUTIONS FOR $Li_{1-x}M_xTi_2O_4$

Composition	Best fit	lnK	u	B_{eff}
$x = 0.00$	$Li_{0.95}[Ti_2]O_4$	0.470	0.2600	0.684
Mg $x = 0.15$	$Li_{0.85}Mn_{0.12}Ti_{0.03}[Ti_{1.97}Mg_{0.03}]O_4$	−0.007	0.2620	1.200
Mn $x = 0.25$	$Li_{0.7}Mn_{0.25}Ti_{0.05}[Ti_{1.95}Li_{0.05}]O_4$	−0.0406	0.2600	1.138
Mn $x = 0.70$	$Li_{0.25}Mn_{0.70}Ti_{0.05}[Ti_{1.95}Li_{0.05}]O_4$	−0.020	0.2600	0.393
Mn $x = 1.00$	$Mn[Ti_2]O_4$	0.015	0.2605	0.585

TABLE II

THEORETICAL AND OBSERVED X-RAY INTENSITIES FOR $LiTi_2O_4$, $Li_{0.85}Mg_{0.15}Ti_2O_4$, $Li_{0.75}Mn_{0.25}Ti_2O_4$, $Li_{0.3}Mn_{0.7}Ti_2O_4$, and $MnTi_2O_4$

	$Li_{0.75}Mn_{0.25}Ti_2O_4$		$Li_{0.3}Mn_{0.7}Ti_2O_4$		$MnTi_2O_4$	
hkl	Obs.	Calc.	Obs.	Calc.	Obs.	Calc.
111	998	839	203	204	76	77
220	87	101	266	266	361	350
311	1000	1000	1000	1000	1000	1000
222	53	77	35	47	35	44
400	770	716	288	321	200	205
331	52	64	—	—	—	—
422	25	26	83	85	106	110
511 + 333	383	350	369	365	355	351
440	648	561	523	617	500	448
531	100	96	24	23	—	—
620	—	—	27	29	33	38
533	70	77	97	92		
622	42	44	34	33		
444	85	83	36	43		
711 + 551	39	47	13	15		
642	—	—	30	39		
731 + 553	104	102	133	143		
800	55	60	67	65		

	$LiTi_2O_4$		$Li_{0.85}Mg_{0.15}Ti_2O_4$	
hkl	Obs.	Calc.	Obs.	Calc.
111	1000	1000	1000	1000
220	5	5	18	18
311	482	469	499	532
222	51	59	43	62
400	733	609	675	582
331	84	96	66	59
511 + 333	214	181	212	211
440	404	337	346	351
531	140	116	106	103
533	43	40	38	44
622	38	36	40	37
444	82	79	76	70
711 + 551	48	56	42	51
731 + 553	66	59	45	64
800	37	41	33	40

magnesium series, a small amount of octahedral Mg^{2+} is suggested. The best fit for the $LiTi_2O_4$ sample shows a lithium deficiency, which is reasonable considering the volatility of Li_2O at the firing temperature. The value of the u parameter for $LiTi_2O_4$ is in good agreement with the results of Johnston ($u = 0.264$, Ref. (*4*)) and Harrison *et al.* ($u = 0.261$, Ref. (*7*)).

In the case of the manganese series the adherence of the lattice parameter to Vegard's law further supports tetrahedral substitution for Mn^{2+} since both end members are considered to be normal spinels; any

deviation from a linear lattice parameter dependence of x would imply that the solid solution does not possess the same extent of normality as the end members. The preference of the M^{2+} cations for the tetrahedral sites is explained largely by the principle of "highest charge neutralization" (*22*). The absence of any net octahedral field stabilization energy for Mg^{2+} or Mn^{2+} (d^5 high spin) is also contributory.

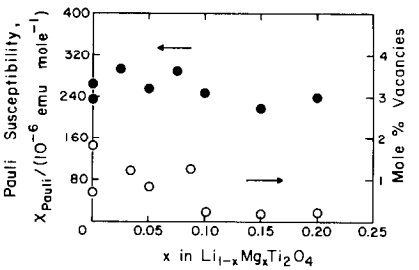

FIG. 4. Compositional variation of χ_{Pauli} and oxygen vacancy concentration for $Li_{1-x}Mg_xTi_2O_4$.

Results

A. Magnetic Susceptibility

The substitution of nonmagnetic Mg^{2+} cations allows investigation of compositional trends in both the Curie-like behavior of the spins trapped at oxygen vacancies and the conduction electron Pauli susceptibility. Representative molar susceptibilities for $x = 0$ and $x = 0.075$ are shown in Fig. 3. Included are fits to the function,

$$\chi_M = C/T + \chi_{Pauli} + \chi_{TD}T, \qquad (6)$$

where χ_M is the molar susceptibility, T is the temperature in degrees Kelvin, C is the Curie constant, χ_{Pauli} is the temperature-independent term reflecting the response of the conduction electrons, and χ_{TD} is the temperature-dependent term similar to that applied to $LiTi_2O_4$ (*4*, *7*).

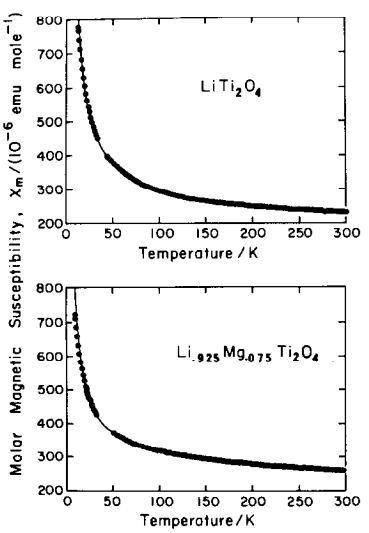

FIG. 3. Representative molar susceptibilities for $Li_{1-x}Mg_xTi_2O_4$ (CGS units).

As outlined elsewhere (*4*, *7*), temperature-dependent terms in the magnetic susceptibility (as exemplified by χ_{TD}) may arise from a variety of sources:

(i) enhancement effects in the Pauli paramagnetism, due to either electron–electron or electron–phonon interactions (*7–10*, *13*, *16*);

(ii) the presence of quasiparticles such as large polarons or mobile spin-paired dimers (*7*).

The χ_{Pauli} term appears relatively insensitive to composition and in the lower x value compositions, the number of vacancies calculated from the Curie constants is independent of the x value (Fig. 4). Similar observations were made by Harrison *et al.* (*7*) and Johnston (*4*) for the $Li_{1+x}Ti_{2-x}O_4$ system. Above $x = 0.1$, the number of vacancies falls significantly and is correlated with the weakening of the ESR vacancy resonance intensity (*13*).

Up to $x = 0.5$ in the $Li_{1-x}Mn_xTi_2O_4$ series, the magnetic susceptibility is dominated by the Curie–Weiss behavior of high-spin Mn^{2+} local moments. In the compositions $x = 0.05$ and $x = 0.1$ the best fits to the data include a temperature-indepen-

TABLE III

MAGNETIC SUSCEPTIBILITY DATA FOR $Li_{1-x}Mn_xTi_2O_4$

x	Temp. (°K)	C	μ_{eff} (μ_B)	θ (°K)	$10^6\chi_{Pauli}$ (emu/mole)	Spontaneous magnetic moment (μ_B)	T_c' (°K)
0.05	12–300	0.191	5.53	9.7	260		
0.10	12–300	0.398	5.65	11.8	277		
0.20	9–300	0.906	6.02	15.7	—		
0.30	7–300	1.351	6.00	19.2	—		
0.40	5–300	1.756	5.93	20.5	—		
0.50	5–300	2.135	5.85	17.7	—		
0.60	200–300	2.618	5.91	21.8	—	0.003	15
0.70	200–300	3.125	5.98	37.4	—	0.07	25
1.00	200–300	3.545	5.33	37.4	—	0.39	55

dent χ_{Pauli} term. For higher x values ($0.10 < x < 0.50$) any temperature-independent term is swamped by the response of the Mn^{2+} moments, and the inverse magnetic susceptibility is completely modeled by a Curie–Weiss law with a slight antiferromagnetic interaction (Fig. 5, Table III). The μ_{eff} values are close to the free spin value of 5.9 μ_B (Fig. 6).

A deviation from Curie–Weiss behavior is observed in x = 0.6 and increased through x = 1.0; the inverse susceptibility is linear only from 150 to 300 K and falls off hyperbolically at lower temperatures (Fig. 7). The μ_{eff} and θ values obtained from the linear Curie–Weiss portion of the inverse susceptibility are included in Table III and Fig. 6. Field dependencies, indicating spontaneous magnetism, are observed in the low-temperature susceptibilities of the x = 0.6, 0.7, and 1.0 compositions. T_c' is the ordering temperature associated with these moments. Saturation could not be achieved at the maximum field of 12,000 G and so the calculated spontaneous moments listed in Table III must be considered as low limits. The possibility of spin glass formation, in which metastable frustrated spin configurations are randomly frozen out at an or-

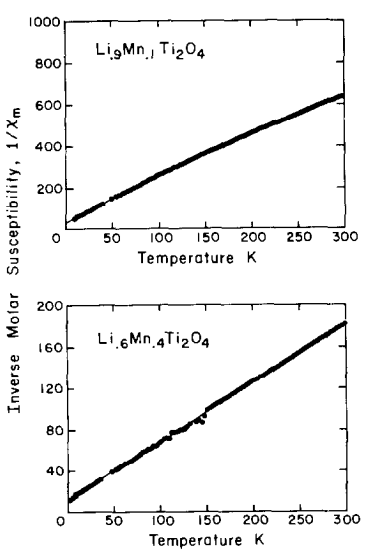

FIG. 5. Representative inverse molar susceptibilities for $Li_{1-x}Mn_xTi_2O_4$, $0 \leq x \leq 0.5$ (CGS units).

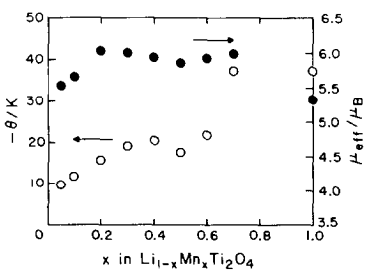

FIG. 6. Effective magnetic moment μ_B and Weiss constant θ for $Li_{1-x}Mn_xTi_2O_4$.

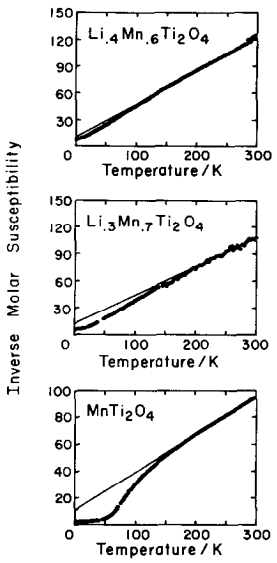

FIG. 7. Inverse molar susceptibilities of the $x = 0.6$, 0.7, and 1.0 compositions of $Li_{1-x}Mn_xTi_2O_4$ indicating ordering at low temperatures.

TABLE IV

SUPERCONDUCTING TRANSITION TEMPERATURES FOR $Li_{1-x}M_xTi_2O_4$

X	T_c (°K)	ΔT_c (°K)
Mg x = 0.0 (No. 1)	10.8	5.9
0.0 (No. 2)	8.9	4.3
0.0 (No. 3)	9.8	4.6
0.025	9.4	4.1
0.05	8.8	4.2
0.075	8.4	4.0
0.10	8.8	4.7
0.15	7.8	4.6
0.20	7.0	4.8
Mn x = 0.05	9.1	4.2
0.1	7.8	4.4
0.15	5.9	3.6
0.2	3.6	3.5
0.25	3.3	2.5

dering temperature, was investigated by field cooling experiments. However, no difference was observed in the susceptibilities obtained from samples cooled in the 12,000 G field and those cooled in zero field.

B. Superconductivity

With five unpaired spins in the *d*-orbital manifold, high-spin Mn^{2+} should act as an effective scattering center providing there is conduction electron density near the impurity. The effects of a magnetic ion on the transition temperature T_c should be substantially greater than that of a nonmagnetic ion such as Mg^{2+}, assuming an equal mean-free path. A comparison of the superconducting properties of the two series therefore provides a measure of the interaction between the conduction electrons and the tetrahedral cation sublattice.

The superconducting transition temperature falls more rapidly in the manganese series (Fig. 8a, Table IV) but not as precipitously as expected for a magnetic impurity effect. A strong correlation is evident between T_c and the cubic lattice parameter across both series (Fig. 8b) where

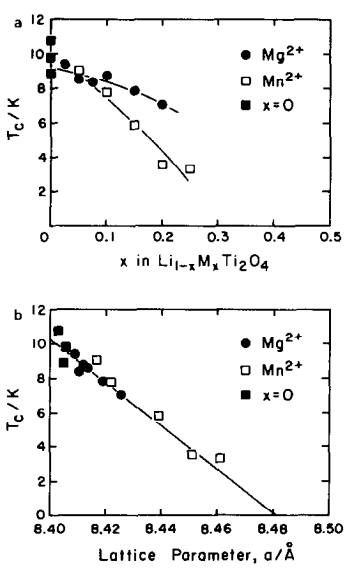

FIG. 8. Superconducting transition temperature T_c in $Li_{1-x}M_xTi_2O_4$, $M = Mn^{2+}$, Mg^{2+}, versus (a) composition x and (b) lattice parameter a.

$$T_c = (1073.7 - 126.6a)°K \quad (7)$$

with a correlation coefficient of −0.974.

The signal amplitude of the superconducting transition temperature falls for the $x = 0.2$ and 0.25 samples of the manganese series. The detection of the transition temperature in the latter composition corresponds to the sensitivity limit of the AC mutual inductance apparatus. The signal amplitude measured by this technique is at best a rough approximation of the volume of superconducting material and is susceptible to grain size and phase distribution effects. It is possible that the superconductivity observed in these compositions mentioned above reflects homogeneity fluctuations or an increased penetration depth λ_L. An increase in λ_L as the insulating composition of $MnTi_2O_4$ is approached is not unreasonable considering the inverse relation between the conduction electron mean-free path and λ_L.

The magnitude and variation of T_c for the $LiTi_2O_4$ samples are similar to previous studies (*4, 7*). The transition widths are large in comparison to other superconductors, but consistent with those found for the $Li_{1+x}Ti_{2-x}O_4$ system by AC mutual inductance (*7*).

Discussion

A. Magnetic Susceptibility

As x increases in the $Li_{1-x}Mg_xTi_2O_4$ series, an enhancement in χ_{Pauli} is expected since (1) the resulting band narrowing increases both the effective mass m^* and the density of states at the Fermi level, $N(E_F)$, and (2) the addition of electrons further increases $N(E_F)$ for a less-than-one-half-filled band. Since an increase in effective mass is inescapable as the band narrows, the general trend in χ_{Pauli} as x increases implies a decreasing $N(E_F)$. This point will be addressed in the next section.

The observation of free-spin Mn^{2+} local moments is consistent with the X-ray line intensity analysis placing the manganese cations at the tetrahedral sites. Since the high-spin d^5 configuration has no angular momentum and, to a first approximation no spin–orbit coupling, a modified Mn^{2+} moment would indicate conduction electron-mediated interactions. Such spin exchange would most reasonably occur on the B sublattice. An unaffected moment does not, however, preclude octahedral site occupation; the Mn^{2+} energy levels could be sufficiently separated from the conduction band to limit spin exchange.

The negative Weiss constants obtained for $x < 0.5$ (Fig. 9) do not imply magnetic ordering, but rather indicate small antiferromagnetic interactions within the magnetic clusters of Mn^{2+} cations or between isolated Mn^{2+} cations. The weak interactions are again consistent with tetrahedral site occupation since the A sites do not share common anions with which to facilitate superexchange. Experimentally, low antiferromagnetic ordering temperatures and Weiss constants are obsrved for systems with magnetic ions only at the A sites (*23–25*). An exemplary system is $Zn_{1-x}Co_xRh_2O_4$ (*24*) where the Co^{2+} cations are confined to the A sites. Weak antiferromagnetic interactions exist at low x values, as indicated by the Weiss constants shown in Fig. 9. Antiferromagnetic ordering is observed for $x > 0.42$ in excellent agreement with Monte Carlo calculations of

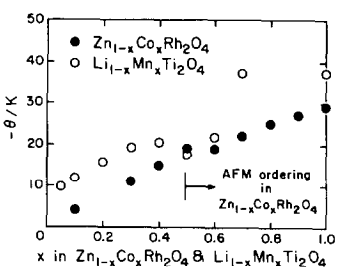

FIG. 9. Compositional variation of θ for $Zn_{1-x}Co_xRh_2O_4$ (*24*) and $Li_{1-x}Mn_xTi_2O_4$.

the A site percolation threshold (*26–28*) assuming only four interacting neighbors. The Weiss constants of the $Li_{1-x}Mn_xTi_2O_4$ series are shown in Fig. 9 for comparison. The manganese series follows the same trend up to $x = 0.4$, after which the incipient antiferromagnetic ordering is frustrated.

In the $x > 0.5$ samples, the hyperbolic shape of the inverse susceptibility and the appearance of spontaneous magnetism at low temperature are not consistent with antiferromagnetic ordering among the A site cations but is characteristic of ferrimagnetic ordering involving local moments on the A and B sublattices. Lecerf *et al.* (*21*) observed spontaneous magnetization in $MnTi_2O_4$ samples at 4.2 and 20.4 K and found the magnetization of the $MnTi_2O_4$ samples varied with the cooling rate after firing. Those samples which were furnace-cooled could not be saturated at 20,000 G, similar to the findings of this study. Although the spin configuration of the ferrimagnetically ordered state can only definitely be established with neutron scattering, "incomplete" saturation is often exhibited in materials with noncollinear spin arrangements; the applied field alters the canting angle of the spins and so increases the net magnetization.

The criteria for a noncollinear arrangement versus a Néel collinear arrangement has been parameterized by Kaplan *et al.* (*29*) in terms of the spin exchange coupling constants for the strongest interactions in the spinel structure, J_{AB} and J_{BB},

$$\mu_{\text{ferri}} = \frac{4J_{BB}S_B}{3J_{AB}S_A} \geq \tfrac{8}{9} \text{ for noncollinear.} \quad (8)$$

In the case of $MnTi_2O_4$, the B–B exchange interaction is substantial because of the strong direct-exchange mechanism between titanium cations. The A–B exchange scales with orbital filling and is weakened for B site cations with less than three d electrons (*30*). Thus, from Eq. (8), a noncollinear configuration is expected for $MnTi_2O_4$, as observed in MnV_2O_4 (*27*) and $MnCr_2O_4$ (*32*) for similar reasons. The lack of a Néel collinear moment of 3 μ_B in $MnTi_2O_4$ is also indicative of a noncollinear arrangement. The ordering persists for compositions of $x \leq 1.0$, where the decreasing Mn^{2+} and Ti^{3+} concentrations reduce the net exchange energy and in doing so lower the transition temperature (Table IV) and magnetization.

In the compositions which ferrimagnetically order, the high-temperature Curie constants should include the effective magnetic contribution from both sublattices. In the case of $x = 0.7$ and 1.0, the Curie constants fail to account for even the full Mn^{2+} moment. Precedent exists for reduced Curie constants in ferrimagnetic spinels with A site manganese. On the basis of a low Curie constant obtained between 300 and 500 K, Dwight *et al.* (*33*) conclude that an intrinsic reduction of the Mn^{2+} moment to $2S = 4.3$ μ_B occurs in $MnCr_2O_4$. To account for the reduced Mn^{2+} moment, the authors assume a full spin-only Cr^{3+} contribution and propose an admixture Mn^{2+} ground state composed of the sextet S state ($^6\phi$) and several quartet states ($^4\phi$),

$$\psi = \alpha^2(^6\phi) + (1 - \alpha^2)^{1/2}(^4\phi), \quad (9)$$

where α is the mixing coefficient. An α value of 0.81 is required to give the observed Curie constant. Neutron diffraction studies in MnV_2O_4 (*31*), $MnCr_2O_4$ (*32, 34*), and $MnFe_2O_4$ (*35*) support the existence of a reduced moment of $2S = 4.3$–4.6 μ_B for Mn^{2+} in the ferrimagnetically ordered state.

An alternative explanation is simply that high-temperature data is required for accurate Curie constants in ferrimagnets. The inverse susceptibilities of several ferrimagnets, including $MnCr_2O_4$ (*36*) and $MnCrAlO_4$ (*37*), show curvature up to 300–400 K before the paramagnetic region is reached. Accordingly, the Curie constant derived in the low-temperature region is

lower than that of the linear high-temperature region. The situation for the $Li_{1-x}Mn_xTi_2O_4$ series may be complicated by a temperature-dependent Ti^{3+} moment from spin-orbit coupling effects.

A complementary description for the fitting of magnetic data from ferrimagnets is outlined by Srinivasan and Seehra (*38*) for the case of hausmannite (Mn_3O_4).

The significance of ordering the $MnTi_2O_4$ is the presence of local moments on the titanium sublattice and the implied insulating state. The appearance of the ordering at $x = 0.6$ suggest a compositionally induced metal–nonmetal transition (MNMT) near that value.

B. Superconductivity

The observation of superconductivity up to $x = 0.25$ in the $Li_{1-x}Mn_xTi_2O_4$ system provides further evidence for tetrahedral Mn^{2+} since, as will be shown in a subsequent paper (*39*), the presence of as little as 2 at.% Cr^{3+} on the titanium sublattice destroys the superconductivity through a magnetic impurity effect.

The Bardeen *et al.* (*40*) theory of superconductivity is reduced to a single expression for the transition temperature,

$$T_c = \theta_D \exp(-1/N(E_F)U_{BCS}), \quad (10)$$

where θ_D is the Debye temperature, roughly a measure of the mean phonon frequency, and U_{BCS} is the attractive electron–lattice interaction.

The correlation of the superconducting transition temperature in the $Li_{1-x}M_xTi_2O_4$ series to lattice parameter appears at first glance to be inconsistent with the behavior predicted by Eq. (10); as x increases, the addition of conduction electrons combined with the concurrent narrowing of the t_{2g} band should increase $N(E_F)$ and thus should similarly increase T_c. (The electron–lattice interaction term, U_{BCS}, should remain fairly insensitive to compositional changes within a given crystal system.)

At a characteristic bandwidth, the above model collapses as electron correlation and electron–lattice interactions are no longer adequately treated as small perturbations to the collective electron Hamiltonian. In the Hubbard formalism (*41*), electron correlation drives a band splitting in a system with an integral number of electrons per atomic site as the MNMT is approached from the broadband limit. The density of states at the Fermi level decreases gradually (Fig. 10) as U_{eff}, the coulomb interaction energy, increases as the limit of complete localization is approached. The band gap at this limit corresponds to a charge transfer energy.

The density of the continuum states is consumed by localized states formed from the increasing electron correlation. Although correlation effects are weakened with more (or less) than an integral number of electrons per atom, the electron–lattice interaction becomes influential as the metal–nonmetal transition is approached and the overall trend in $N(E_F)$ remains the same.

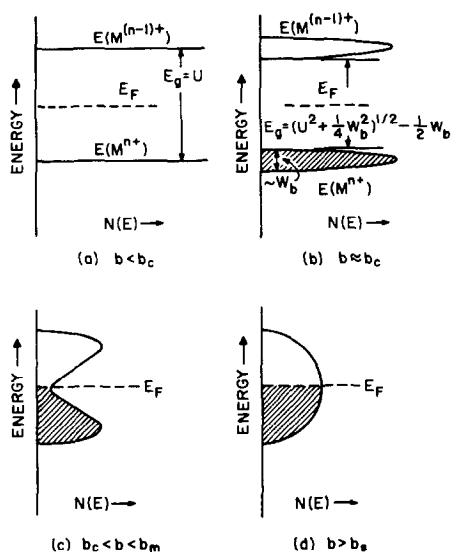

FIG. 10. Schematic representation of the decrease in the Fermi level density of states $N(E_F)$ with increasing U_{eff}, modified from Ref. (*45*).

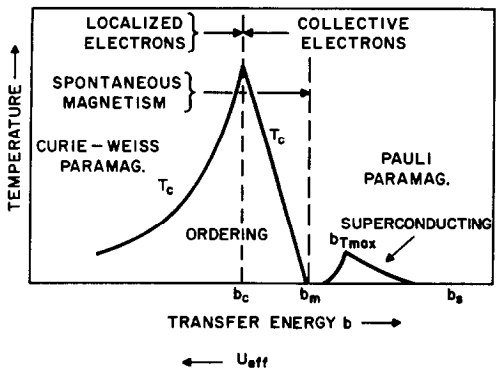

FIG. 11. Qualitative temperature versus bandwidth phase diagram detailing magnetic and electronic states (modified from (*42*, *45*)).

The dependence of T_c for a superconductor on bandwidth is phenomenologically described by Goodenough (*42*). The bandwidth B is related to b, the overlap or transfer energy, as

$$B = 2zb \tag{11a}$$

$$b_{ij} = (\psi_i H \psi_j), \tag{11b}$$

where z is the number of like nearest neighbors. As shown schematically in Fig. 11, a superconducting state in the collective electron regime displays the following behavior. As b decreases from the broadband limit, T_c gradually increases via an increase in $N(E_F)$. As the band narrows further, T_c is maximized and, assuming the BCS model is still applicable in this regime, begins to fall as electron correlation (the Hubbard U_{eff} is nonzero) and the electron–lattice interactions (the atomic cores are no longer screened effectively) reduce the density of states at the Fermi level. It is important to note that the complete loss of superconductivity occurs well before the MNMT.

$LiTi_2O_4$ is certainly in the narrow-band regime and the electron–lattice interactions are strong, based on the calculated electronic mean-free path of 11.2 Å (*8*) and the high superconducting transition temperature. It is not unreasonable to place the transfer energy at b_{Tmax}. Since the narrowing of the bandwidth or transfer energy scales approximately with lattice parameter, the transition temperature falls smooothly and linearly with the decreasing density of states, as x increases in $Li_{1-x}M_xTi_2O_4$. The extrapolated $T_c = 0$ K composition is $x = 0.35$, well before the MNMT, in agreement with Goodenough's phase diagram. The χ_{Pauli} values for the magnesium series qualitatively support a decrease in $N(E_F)$.

Conclusions

In a strict sense, the formal arguments of the Mott (*43*) and Wigner (*44*) models are not appropriate to the MNMT observed in the $Li_{1-x}Mn_xTi_2O_4$ system since there is a nonintegral number of electrons per titanium ion at the transition. Thus, the driving force for the MNMT cannot be wholly electron correlation. Nevertheless, such effects are likely to be present as the titanium–titanium distance is increased, in addition to the strong electron–lattice interactions.

The existence of a nonintegral number of electrons per atomic site alters the physical manifestation of the transition. In the Mott model, a sharp transition is expected as the reduction in screening by the conduction electrons further encourages localization, the vice versa. With a nonintegral number of electrons per atomic site, the degeneracy of the charge transfer

$$M^{+n} + M^{+(n+1)} \rightarrow M^{+(n+1)} + M^{+n} \tag{12}$$

is maintained, and the electrons are free to move through the lattice. However, the electron–lattice interaction confers upon the electron an envelope of atomic displacement and the volume of this quasiparticle, or polaron, decreases with increasing electron–lattice interaction. In the metallic regime, large polarons with associated atomic displacements extending over sev-

eral unit cells comprise the continuum band states. In the small polaron unit, the lattice displacements are limited to the immediate atomic sites and the electron resides in the localized state.

At a given temperature, a critical cation–cation separation will distinguish the continuum band mobility of large polarons from the activated mobility of the small polarons in the insulating state. Goodenough (*45*) has proposed a semiempirical criterion for this distance R_c in transition metal oxides with strong cation–cation interactions.

$$R_c = \{3.20 - 0.05m - 0.04S_i(S_i + 1) - 0.03(Z - Z_{Ti})\}\ \text{Å}, \quad (13)$$

where m is the valence state of the cation, S_i is the electron spin, and Z is the atomic number of the cation. All three parameters mimic the reduction in the radial extension of the d orbitals across the periodic table. By the appearance of magnetic order, the MNMT in $Li_{1-x}Mn_xTi_2O_4$ is placed approximately at $x = 0.6$ which corresponds to a Ti–Ti separation of 3.016 Å, in excellent agreement with the R_c value of 3.02 Å for Ti^{3+} from Eq. (13).

Acknowledgments

We thank Sandra Issler for the powder diffractometer measurements. This research was sponsored by the Air Force Office of Scientific Research, NSF, the Material Science Center at Cornell University, and NATO. P.M.L. also acknowledges an ARCO Doctoral Fellowship. P.P.E. thanks the Nuffield Foundation for the award of a Research Fellowship.

References

1. A. Deschanvres, B. Raveau, and Z. Sekkal, *Mater. Res. Bull.* **6,** 699 (1971).
2. D. C. Johnston, H. Prakash, W. H. Zachariasen, and R. Viswanathan, *Mater. Res. Bull.* **8,** 777 (1973).
3. D. C. Johnston, Ph.D. Thesis, University of California, San Diego (1975).
4. D. C. Johnston, *J. Low Temp. Phys.* **25,** 145 (1976).
5. R. W. McCallum, D. C. Johnston, C. A. Luengo, and M. B. Maple, *J. Low Temp. Phys.* **25,** 177 (1976).
6. M. R. Harrison, Ph.D. Thesis, Oxford University (1981).
7. M. R. Harrison, P. P. Edwards, and J. B. Goodenough, *J. Solid State Chem.* **54,** 136 (1984).
8. M. R. Harrison, P. P. Edwards, and J. B. Goodenough, *Philos. Mag. B.* **52,** 679 (1985).
9. P. P. Edwards, R. G. Egdell, I. Fragala, J. B. Goodenough, M. R. Harrison, A. R. Orchard, and E. G. Scott, *J. Solid State Chem.* **54,** 127 (1984).
10. M. R. Harrison, P. P. Edwards, and J. B. Goodenough, *J. Solid State Chem.* **54,** 426 (1984).
11. T. Inukai and T. Murakami, *Japan J. Appl. Phys.* **22** (Suppl. 22-2), 61 (1983).
12. B. Morosin and J. C. Mikkelson, *Acta Crystallogr. Sect. B* **25,** 798 (1979).
13. P. M. Lambert, Ph.D. Thesis, Cornell University (1986).
14. H. Furuhashi, M. Inagaki, and S. Naka, *J. Org. Nucl. Chem.* **35,** 3009 (1973).
15. K. Yvon, W. Jeitschko, and E. Parthe, *J. Appl. Crystallogr.* **10,** 73 (1977).
16. D. C. Johnson, Ph.D. Thesis, Cornell University (1983).
17. A. Lecerf, *Ann. Chim.* **7,** 513 (1962).
18. V. T. Dension, S. I. Kobeleva, A. I. Korosteleva, V. V. Shevchenko, and V. F. Shuvalov, *Kinet. Katal.* **24,** 168 (1983).
19. U. Roy, A. Das Gupta, and C. C. Koch, *IEEE Trans. Magn.* **13,** 1 (1977).
20. A. H. Mousa and N. W. Grimes, *J. Mater. Sci.* **15,** 793 (1980).
21. A. Lecerf, M. Rault, and G. Villers, *C. R. Acad. Sci. (Paris)* **261,** 749 (1965).
22. E. J. W. Verwey and E. L. Heilmann, *J. Chem. Phys.* **15,** 174 (1974).
23. W. L. Roth, *J. Phys. Rad.* **25,** 507 (1964).
24. G. Blasse, *Philips Res. Rep.* **18,** 383 (1963).
25. G. Blasse and D. J. Schipper, *Phys. Lett.* **5,** 300 (1963).
26. D. Fiorani and S. Viticoli, *Solid State Commun.* **29,** 239 (1979).
27. D. Fiorani and S. Viticoli, *J. Phys. Chem. Solids* **41,** 959, 1041 (1980).
28. D. Fiorani, S. Viticoli, and G. A. Korteveg, *Solid State Commun.* **36,** 89 (1980).
29. T. A. Kaplan, K. Dwight, D. H. Lyons, and N. Menyuk, *J. Appl. Phys.* **32,** 135 (1961).
30. J. B. Goodenough, "Magnetism and the Chemical Bond," Interscience, New York (1963).

31. R. PLUMIER, Ph.D. Thesis, Paris (1968).
32. S. VRATISLAV, J. ZAJICEK, AND A. F. ANDRESEN, *J. Magn. Magn. Mater.* **5,** 41 (1977).
33. K. DWIGHT, N. MENYUK, J. FEINLEIB, AND A. WOLD, *J. Appl. Phys.* **37,** 962 (1966).
34. A. J. HEEGER AND T. W. HOUSTON, *Proc. Int. Conf. Magn., Nottingham,* 395 (1964).
35. J. M. HASTINGS AND L. M. CORLISS, *Phys. Ref.* **104,** 328 (1956).
36. T. R. MCGUIRE, L. N. HOWARD, AND J. S. SMART, *Ceram. Age* **60,** 22 (1952).
37. P. L. EDWARDS, *Phys. Rev.* **116,** 294 (1959).
38. G. SRINIVASAN AND M. S. SEEHRA, *Phys. Rev. B.* **28,** 1 (1983).
39. P. M. LAMBERT, M. R. HARRISON, AND P. P. EDWARDS, submitted for publication (1988).
40. J. BARDEEN, L. N. COOPER, AND J. R. SCHRIEFFER, *Phys. Rev.* **108,** 1175 (1957).
41. J. HUBBARD, *Proc. R. Soc. London Ser. A* **281,** 401 (1965).
42. J. B. GOODENOUGH, *Prog. Solid State Chem.* **5,** 291 (1971).
43. N. F. MOTT, *Proc. R. Soc. London Ser. A* **62,** 416 (1949).
44. E. WIGNER, *J. Chem. Soc. Faraday Trans. I* **34,** 678 (1938).
45. J. B. GOODENOUGH, *Czech. J. Phys. B* **17,** 304 (1967).